ORNL/TM-2016/179

Improved Structural Design and CO_2 Capture of Porous Hydroxy-Rich Polymeric Organic Frameworks

Michelle K. Kidder
Valmor F. de Almeida
Lyndsey D. Earl

16 August 2016

OAK RIDGE NATIONAL LABORATORY
MANAGED BY UT-BATTELLE FOR THE US DEPARTMENT OF ENERGY

Improved Structural Design and CO_2 Capture of Porous Hydroxy-Rich Polymeric Organic Frameworks*

Michelle K. Kidder, Lyndsey D. Earl, and Valmor F. de Almeida

Chemical Sciences Division
Oak Ridge National Laboratory
Oak Ridge, TN 37831-6119, USA

Technical Report ORNL/TM-2016/179

16 August 2016

*Also available by request to kidderm@ornl.gov

Abstract

Polymeric organic frameworks (POFs) are tunable and robust porous materials with potential applications for gas capture, catalysis, and separations technologies. A series of new porous POFs have been synthesized from the reaction of phloroglucinol or resorcinol derivatives with aryl aldehyde precursors. The monomers have various molecular shapes including linear, bent, trigonal, and tetrahedral geometries. Depending on the size and geometric matching of the monomers, the polymers are dominantly microporous with some mesoporous character or they are non-porous. In addition to standard spectroscopic and surface characterization, the materials were screened as adsorbents for carbon dioxide capture at low pressure (0-1 bar). The best performing material (**POF 1D**) has a CO_2 capture capacity of 9.0 wt. % (2.04 mmol g^{-1}) at 298 K and 1 bar which is comparable to other polymeric organic frameworks. Isosteric heats of adsorption for **POF 1A**, **POF 2A**, and **POF 2B** were found to be dependent on the weight percent of CO_2 adsorbed: this suggests there are both chemisorptive and physisorptive components of CO_2 capture by the POFs.

Contents

List of Figures

List of Schemes

List of Tables

1 Introduction

Cost effective capture of carbon dioxide from anthropogenic sources for utilization and storage requires the use of adsorbents that are as energetically efficient as possible. Additionally, since the atmospheric levels of carbon dioxide have reached and surpassed the 400 ppm level, devising even more efficient methods for direct air capture (Choi *et al.*, 2011; Lu *et al.*, 2013) and removing carbon dioxide from industrial flue gas (Lee and Park, 2015; Liu *et al.*, 2012) before it ever enters the atmosphere is of increasing relevance. The current technology for removing carbon dioxide from coal fired or natural gas power plant exhaust is scrubbing with monoethanolamine solutions. These amine solutions are corrosive, eventually degrade, and require about 30 % of a power plant's energy to regenerate the adsorbed carbon dioxide and recycle the adsorbent liquid.

In the quest for alternative technologies to monoethanolamine scrubbers, researchers have turned to porous materials as adsorbents for post-combustion carbon capture. Some of the best reported porous materials for carbon dioxide capture includes a nitrogen-doped carbon monolith (Ma *et al.*, 2014) with CO_2 capacities of 8.99 mmol g^{-1} at 273 K and 1 atm and, more relevantly, 1.51 mmol g^{-1} at 298 K and 0.15 atm. A microporous metal-organic framework (MOF) containing triazole and pyridine functionalities has a CO_2 uptake capacity of 6.1 mmol g^{-1} at 298 K and 1 bar (Lässig *et al.*, 2011). In the realm of porous materials as potential adsorbents for CO_2 capture, zeolites and MOFs have received the bulk of the attention because of their high surface areas and well-established structures.

Recently, a growing amount of consideration has been given to polymeric organic framework (POF) materials (Budd *et al.*, 2004; McKeown and Budd, 2006; Yuan *et al.*, 2011). POFs are amorphous organic polymers that are insoluble in water and common organic solvents. Some of the benefits of polymeric organic frameworks over metal-organic frameworks and zeolites include stability under acidic and basic conditions, heat, and atmospheric moisture, all of which are characteristics of industrial flue gas. Like crystalline MOFs and covalent-organic frameworks (COFs), (Ding and Wang, 2013; Farha *et al.*, 2012) POFs have remarkable promise for adsorption, catalysis, and separations applications because of the ease of synthesis, accessible surface areas, chemical functionality, and structural integrity of these materials (Gao *et al.*, 2014; Katsoulidis and Kanatzidis, 2011; Kaur *et al.*, 2011; Li and Wang, 2013).

Researchers strive to use rational design to predictively synthesize materials with known porosities, (Zhang *et al.*, 2014a; Zou *et al.*, 2013) and some work has shown the size and geometry of the monomers influences the surface area and porosity of the final polymer (Pei *et al.*, 2014; Stockel *et al.*, 2009; Yuan *et al.*, 2011). For example, POFs with dendritic precursors (Zhang *et al.*, 2014b) have improved sur-

face areas while higher specific surface areas and pore volumes are obtained with non-linear linkers than with linear precursors (MA *et al.*, 2012). Microporous materials for hydrogen storage and carbon dioxide capture have been formed through the benzoin condensation of tris-benzaldehydes of various sizes (ZHAO *et al.*, 2012). Previous research suggests tetrahedral monomers prevent the close packing and structural collapse of polymers which help to ensure accessible surface areas and greater pore volumes (LI *et al.*, 2014a,b).

Our approach for synthesizing new hydroxy-rich POFs expands upon reports of a polymer formed from the reaction of phloroglucinol and terephthalaldehyde (KATSOULIDIS AND KANATZIDIS, 2011). Polymers embedded with phloroglucinol and resorcinol derivatives are attractive because the hydroxy groups within the POFs have more favorable physical adsorption of gases like CO_2 through an enhanced dipole-quadrupole interaction (GASSENSMITH *et al.*, 2011). Few examples of porous POFs containing a significant number of -OH groups have been reported. A study of a cyclic-oligosaccharide Rb-MOF with intrinsic hydroxy groups suggests CO_2 chemisorbs to -OH groups to form the observed carbonic acid at very low pressures (ca. 1 Torr) (GASSENSMITH *et al.*, 2011). A Zn-MOF with -OH groups incorporated in the organic linker has a reduced BET surface area but increased CO_2 uptake compared to the Zn-MOF without the -OH functionality (LING *et al.*, 2012).

In this work, the synthesis, characterization, and CO_2 capture capacity of a series of hydroxy-rich POFs made from rigid aryl monomers of various geometries and sizes will be presented. The influence of monomer shape on the surface area, pore diameter, pore volume, and CO_2 capacity of these POFs will be addressed. Precursors with resorcinol functionality provide the same benefits as phloroglucinol but with expanded geometric and synthetic versatility.

2 Experimental

2.1 Materials

Phloroglucinol, terephthalaldehyde, tris(4-formylphenyl)amine, $Pd(dppf)Cl_2 \cdot CH_2Cl_2$, 4-formylphenylboronic acid, 3,5-dimethoxyphenylboronic acid, $CDCl_3$, and $(CD_3)_2CO$ were purchased from Sigma-Aldrich and used as received. 1,4-Dioxane d_8 was purchased from Cambridge Isotope Laboratories. 5'-(3,5-Dihydroxyphenyl)-3,3'',5,5''-tetrahydroxy-1,1':3',1''-terphenyl,(CHAUMONT *et al.*, 2013) tetrakis(3',5'-dihydroxy-[1,1'-biphenyl]-4-yl)methane,(CHAUMONT *et al.*, 2013) [1,1':3',1''-terphenyl]-4,4''-dicarboxaldehyde(KUHNERT *et al.*, 2005), 1,3,5-tris(4-bromophenyl)benzene,(SIMALOU *et al.*, 2014) and tetrakis(4-formylphenyl)methane(FOURNIER *et al.*, 2003) were synthesized according to literature procedures. The syntheses of tetrakis(4'-formyl-

[1,1'-biphenyl]-4-yl)methane and 5''-(3',5'-dihydroxy[1,1'-biphenyl]-4-yl)-[1,1':4',1'':-3'',1''':4''',1''''-quinquephenyl]-3,3'''',5,5''''-tetrol are described in the Supporting Information.

2.2 Methods

^{1}H and ^{13}C NMR solution state spectra were collected on a 9.4 T Bruker Avance spectrometer at 400 MHz and 100 MHz, respectively, and referenced to residual solvent (^{1}H: 7.27 ppm ($CDCl_3$), 2.05 ppm ($(CD_3)_2CO$)); ^{13}C: 77.16 ppm ($CDCl_3$), 29.92 ppm ($(CD_3)_2CO$)). ^{13}C solid state NMR spectra were collected on a 9.4 T Bruker Avance spectrometer at 100 MHz with a 3.2 mm MAS probe spinning at 15 kHz. Chemical shifts were referenced to the -CH_3 signal (17.5 ppm) of hexamethylbenzene. Diffuse reflectance spectra were collected on a Cary 5000 UV-Vis-NIR spectrometer (0.1 sec scan^{-1}, 600 nm sec^{-1}) equipped with Cary 5000 Internal Diffuse Reflectance accessory. Spectra are referenced to a polytetrafluoroethylene (PTFE) plate. FT-IR spectra were collected on a Digilab FTS 7000 Series spectrometer (4 cm^{-1} resolution, 32 scans) equipped with a diamond crystal ATR cell. Thermogravimetric analyses were conducted with 10-15 mg sample on a TA Instruments Q5000 at a rate of 10 ℃ min^{-1} under argon at a flow rate of 25 mL min^{-1}. Scanning electron microscopy (SEM) images were obtained on a Hitachi HF-2000 microscope with an accelerating voltage of 8-16 keV. Nitrogen isotherms were measured on a Quantachrome Autosorb-1 analyzer at 77 K. Samples (approximately 30 mg) were treated at 130 ℃ under vacuum until the material had an outgas rate no greater than 15 μmHg min^{-1} (4-16 hours). Brunauer-Emmett-Teller (BET) surface areas (SA_{BET}) were obtained for materials with values in the range of $P/P_0 = 0.01 - 0.07$ (microporous materials) or $P/P_0 = 0.10 - 0.20$ (non-microporous materials) (Bae *et al.*, 2010; Rouquerol *et al.*, 2007; Thommes *et al.*, 2015). These ranges were verified by plotting P/P_0 vs. $V(1 - P/P_0)$ and ensuring only values of P/P_0 below the maximum of $V(1 - P/P_0)$ were used. Total pore volume (V_{total}) and pore size distributions were calculated from a non-local density functional theory (NLDFT). A carbon equilibrium transition kernel at 77 K based on a slit-pore model for pore widths < 20 Å and a cylindrical-pore model for pore widths > 20 Å was used. The micropore volume (V_{micro}) was estimated from the pore volume at $P/P_0 = 0.18$ which corresponds to pores with diameters less than 20 Å. Gravimetric CO_2 isotherms were obtained with a Hiden Analytical Intelligent Gravimetric Analyzer. Samples were treated under vacuum at 130 ℃ overnight prior to analysis.

2.3 POF synthesis

The details for each POF synthesis, including reagent amounts, solvent volume, and yield, are located in Table A.1.

In a typical procedure for the synthesis of **POFs 1A-1E**, the phloroglucinol precursor **1** (0.40-4.0 mmol) and aldehyde precursor (**A-E**, 0.15-3.0 mmol) were dissolved in anhydrous 1,4-dioxane (3-6 mL). The solution was stirred under argon at 70 ℃ for one hour. The solution was transferred to a Teflon-lined reactor, flushed with argon, sealed, and placed in a 220 ℃ oven. After four days, the reactor was removed from the oven and cooled to room temperature. The solid was filtered, washed with THF (4 × 10 mL) and dried *in vacuo* at 120 ℃ overnight (12-16 hours). A red, brown, or black powder was recovered in 71-90 % yield.

In a typical procedure for the synthesis of **POFs 2A-4E**, the resorcinol precursor (**2-4**, 0.13-0.58 mmol) and aldehyde precursor (**A-E**, 0.060-0.44 mmol) were dissolved in anhydrous 1,4-dioxane (3-6 mL). The solution was transferred to a Teflon-lined reactor, flushed with argon, sealed, and placed in a 220 ℃ oven. After four days, the reactor was removed from the oven and cooled to room temperature. The solid was filtered, washed with THF (4 × 10 mL), and dried *in vacuo* at 120 ℃ overnight (12-16 hours). A red, brown, or black powder was recovered in 28-91 % yield.

3 Results and Discussion

Figure 3.1 shows the molecular structures of the monomers used in the syntheses of hydroxy-rich polymeric organic frameworks. Precursors with linear (**A**), bent (**C**), trigonal (**1**, **2**, **3**, **B**), and tetrahedral (**4**, **D**, **E**) geometries were chosen to see how monomer geometry would affect the BET surface area, pore size distribution, pore volume, and carbon capture capacity of the polymers. Additionally, monomers of similar molecular shape but different size (e.g **2** versus **3**, **D** versus **E**) were chosen to observe the influence of extending the phenyl linkage on the surface area and pore properties of the POFs.

Phloroglucinol (**1**) or resorcinol precursors (**2-4**) were reacted with aldehyde precursors **A-E** through electrophilic aromatic substitution and elimination of water to form 20 various POFs (**POFs 1A-4E**), 18 of which are new in the literature. Scheme 3.1 shows an overview of the reaction to form the POFs using **POF 1A** as an example. The monomers are heated at 70 ℃ for one hour and at 220 ℃ for 3-4 days. Treating the solution at 220 ℃ completes the gelation and curing processes, and the polymer formed is a porous powder.

When the mixture of phloroglucinol **1** and terephthalaldehyde **A** are stirred at 70 ℃ in 1,4-dioxane for one hour, molecules such as intermediate **X** (Scheme 3.1)

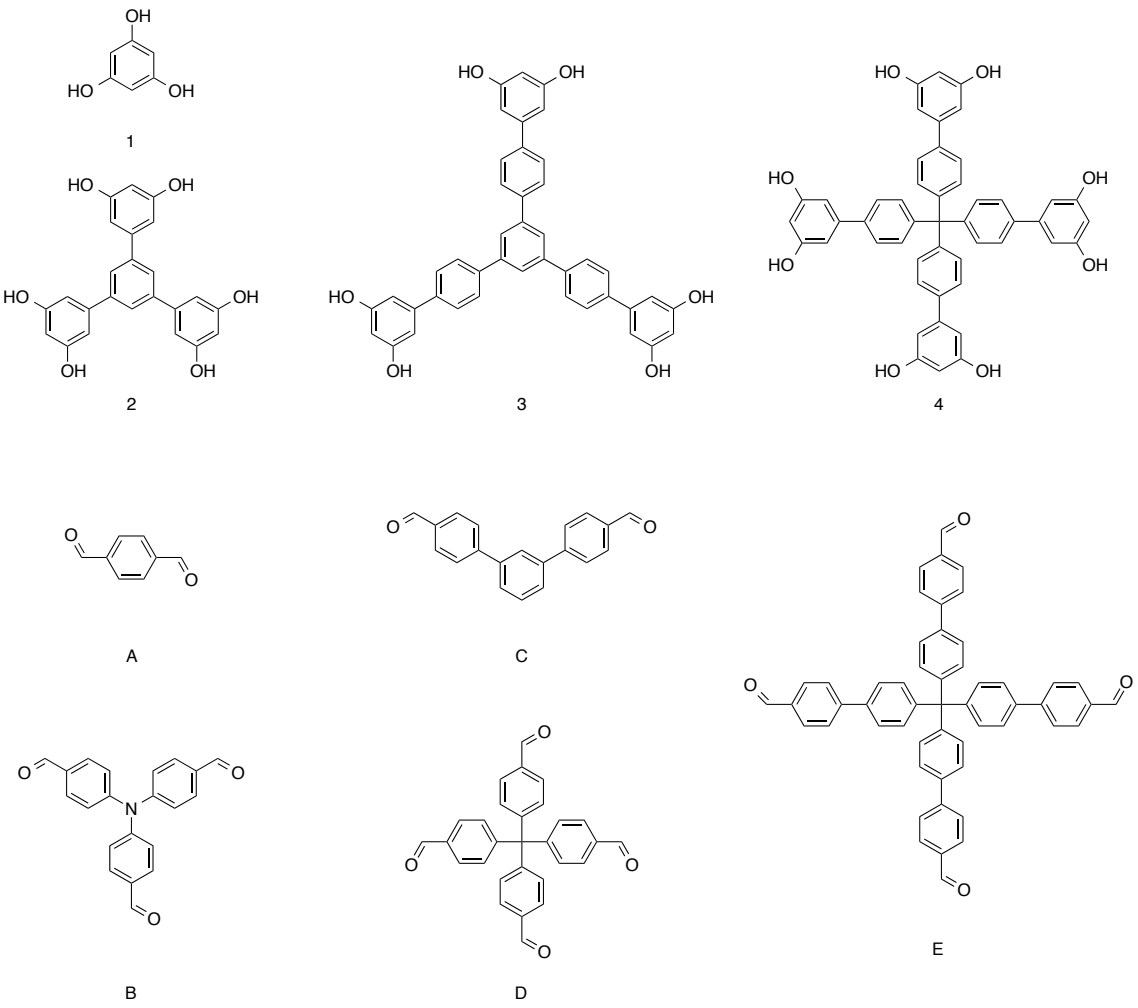

Fig. 3.1: *Molecular structures of phloroglucinol (**1**), resorcinol precursors (**2-4**), and aldehyde precursors (**A-E**) used in the syntheses of **POFs 1A-4E**.*

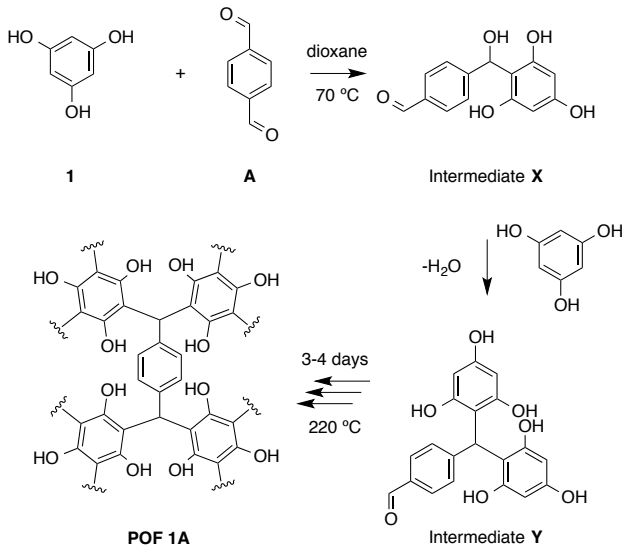

Scheme 3.1: *Monomers **1** and **A** form **POF 1A** via electrophilic aromatic substitution and loss of water when treated at 220 ℃.*

are observed by NMR spectroscopy (see Figure B.1). Previous research suggests heating the reaction mixture at 70 ℃ for one hour improves the yield and surface area properties by "facilitating the mixing of monomers(KATSOULIDIS AND KANATZIDIS, 2011)." Interestingly, the formation of intermediate oligomers is not observed when resorcinol precursors (**2**-**4**) are used instead of phloroglucinol (**1**).

Unsurprisingly, the prescribed pre-treatment with resorcinol precursors rather than phloroglucinol at 70 ℃ does not propagate the formation of oligomers. In fact, reaction mixtures containing **2**-**4** and benzaldehyde precursors do not generate a detectable amount of oligomeric intermediates on the time frame of one hour until the solution is brought to over 200 ℃. Figure B.2 shows the ^{1}H NMR spectrum of a reaction mixture of **2** and **A** in dioxane-d_8 after treatment at 220 ℃ for one hour. The reaction mixture does not appear to proceed along as far compared to the reaction progress made with **1** and **A** at 70 ℃ (Figure B.1). A slow rate of polymerization may help in the controlled microporous solids using structurally diverse monomers.

Equation 3.1 describes the reasoning behind the chosen stoichiometry for the monomers in the POF syntheses. As an example, a molar ratio of 4:3 **1**:**A** is used to ensure the full condensation of **POF 1A** occurs. To form the trityl carbon in **POF 1A** (intermediate **Y**, Scheme 3.1), every carbonyl carbon of **A** reacts with two nucleophilic carbon centers provided by **1**. Therefore, for every mole of **A** (which contains two moles of aldehyde), $\frac{4}{3}$ moles (which contains four moles of carbon centers)

of **1** are required to form a fully condensed polymer **POF 1A**.

$$\frac{\text{mole } \mathbf{1}\text{-}\mathbf{4}}{\text{mole } \mathbf{A}\text{-}\mathbf{E}} = \frac{2 \times \#\text{ aldehydes in } \mathbf{A}\text{-}\mathbf{E}}{\#\text{ sites in } \mathbf{1}\text{-}\mathbf{4}} \tag{3.1}$$

The ratio of the monomers in the syntheses of **POFs 2A-4E** was adjusted such that one available carbon site of the resorcinol moiety (preferably the *para* position) would react with an aldehyde. This was chosen in part to reduce steric crowding around the hydroxy groups and to form interconnected and structurally robust polymers with greater free volume than the **POF 1A-1E**. Looking at Equation 3.1, a value of 3 is used for the number of sites in **2** and **3** and a value of 4 is used for the number of sites in **4**.

The amorphous POFs were characterized using a suite of spectroscopic, thermometric, and imaging techniques. ^{13}C solid state NMR spectra (see Figure B.3) of the polymers verifies the materials are fully condensed. Figure 3.2 shows the ^{13}C solid state NMR spectral assignments of **POF 4A** as an example of what chemical shifts belong to what chemical features of the polymer. There is evidence for a minimal amount of unreacted aldehyde (ca. 192 ppm), and no peaks are present that could be assigned to a secondary alcohol intermediate (ca. 71 ppm). Carbons next to hydroxy groups have resonances at 153-156 ppm for both the phloroglucinol and resorcinol moieties. Aromatic C-H carbons not in close proximity to hydroxy groups have resonances at 128-130 ppm. Unsubstituted *ortho* and *para* carbons of the resorcinol moieties have chemical shifts at 103-108 ppm, while substituted sites have ^{13}C resonances at 110-115 ppm. The quaternary carbon peak at 65 ppm is found in POFs containing precursors **4**, **D**, and **E**. The trityl carbon peak at 35 ppm is broad but also has distinct features. This suggests the carbon center exists in multiple chemical environments and conformations. Although the POFs were dried before analysis, trapped residual solvent is present in the NMR spectra of some of the polymers (1,4-dioxane: 67 ppm; THF: 25 ppm, 68 ppm).

The infrared spectra of the POFs (Figure B.4) shows the characteristic aldehyde C=O stretch near 1700 cm^{-1} is either weak or not present. The aldehyde peak is more apparent in polymers containing precursor **E**. Broad features at 3000–3500 cm^{-1} are assigned to weakly hydrogen bonded hydroxy groups while aromatic -OH out of plane deformations are found at 600-680 cm^{-1}. The strong peaks at 800-850 cm^{-1} are assigned to C-H vibrations of *para*-disubstituted and 1,3,5-trisubstituted benzene units, and peaks at 700-710 cm^{-1} found in the spectra containing precursor **C** are assigned to meta-disubstituted benzene units. All of the POFs have stretches at 1150-1220 cm^{-1} that are indicative of phenolic C-O stretching, and POFs containing tertiary amine **B** display a C-N stretch at 1315-1325 cm^{-1}.

Thermogravimetric analyses (Figure B.5) were conducted to determine the thermal stability of the POFs. The polymers are quite resilient; they are thermally stable

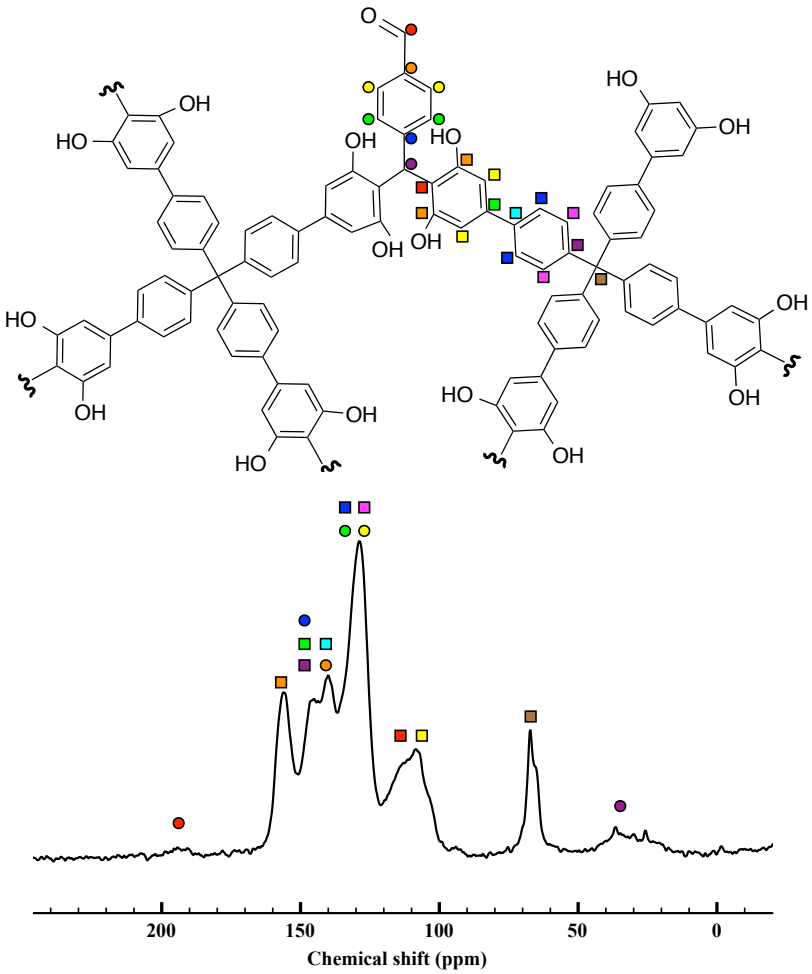

Fig. 3.2: *Assignment of the* ^{13}C *NMR resonances in* ***POF 4A****. The molecular structure shown is a proposed fragment that highlights both fully condensed and unreacted aldehyde features.*

up to 350-400 ℃. At least half of the POF mass remains after being heated to 800 ℃ under argon. The weight loss at temperatures below 150 ℃ is assigned to the loss of residual solvent trapped within the materials' pores and adsorbed atmospheric water vapor. An extended three-dimensional structure and high degree of polymer cross-linking causes the superior thermal stability of the polymers.

The UV-Vis-NIR diffuse reflectance spectra of the POFs is shown in Figure B.6. The material absorbs strongly in the UV region, and additional electronic structure is present at 500 nm in **POFs 1A**, **2A**, and **4C**. NIR absorption tails off at wavelengths greater than 800 nm. The conjugated aryl backbone causes the polymers to have colors ranging in shades of red or brown, and black for polymers that include nitrogen-containing precursor **B**.

SEM imaging of the synthesized POFs (Figure B.7-B.10) shows most of the polymers are semi-regular 1-3 μm particles. Particles of **POF 3C** span both the 1-3 μm and 10-20 μm regime. POFs containing precursor **E** are fibrous and are of similar to the morphology of the tetraaldehyde starting material, though **POFs 1E** and **4E** have a mixed fibrous-nodule morphology. In **POF 1E**, there is a mixture of fibers and interspersed spherical microparticles whereas in **POF 4E**, nodules are embedded in the fibers. While no correlation between the polymer's particle size and micro- or mesoporosity has been found in resorcinol-formaldehyde aerogels (a class of materials similar to **POFs 1A**-**4E**),(Horikawa *et al.*, 2004) the fiber morphology of polymers containing **E** suggests the monomer may never fully dissolve in the reaction solution. Additionally, spectroscopic evidence (IR and NMR, *vide supra*) exists for a prevalence of unreacted aldehyde in POFs made of monomer **E** which further supports that the solubility of **E** influences the macroscopic structure of **POFs 1E**-**4E**.

3.1 Surface Area and CO_2 Capture Properties

Pore volume, pore size distribution, and accessible surface area are important metrics for carbon dioxide physiosorption and other potential applications of POFs. Nitrogen adsorption and desorption isotherms were collected for **POFs 1A**-**4E** between $P/P_0 = 10^{-6} - 1$ at 77 K (Figure 3.3). Most of the POFs have nitrogen isotherms with varying ultra-microporous (pore diameter < 7 Å), microporous (< 20 Å), and mesoporous (20-500 Å) contributions and modest (400-1300 $m^2\ g^{-1}$) surface areas for amorphous organic polymers. Few of the POFs are non-porous, namely **POFs 2C**, **3A**, **3C**, and **3D**, and only exhibit weak adsorbent-adsorbate interactions. The low surface areas and lack of porosity in these POFs can be attributed to a number of factors: π-stacking of the polymer forms pores that are too small to detect by N_2 adsorption at 77 K, severe structural collapse transpired upon solvent removal, or geometric and size mismatching of the organic monomers occurred.

Table 3.1: *BET surface area, micropore volume[b], total pore volume, and predominant pore size of* ***POFs 1A-4E****.*

POF	SA_{BET} (m^2 g^{-1})	V_{micro} (cm^3 g^{-1})[b]	V_{total} (cm^3 g^{-1})	Pore size (Å)	CO_2 uptake[c] (wt.%)
1A	688	0.29	0.43	6, 12	5.9
1B	502	0.24	0.47	7, 13	3.6
1C	175[a]	0.068	0.20	12	4.3
1D	641	0.26	0.32	6, 13, 19	9.0
1E	914	0.39	0.60	6, 11-17	4.3
2A	533	0.23	0.43	6-7, 12	7.2
2B	750	0.30	0.53	6-7, 13	8.1
2C	12[a]	0.002	0.018	N/A	3.8
2D	672	0.30	0.54	7-10, 13, 19	4.4
2E	370[a]	0.15	0.32	10, 12	6.8
3A	31[a]	0.004	0.042	N/A	6.1
3B	325	0.14	0.19	7, 13, 19	7.5
3C	15[a]	0.003	0.020	N/A	3.3
3D	9[a]	0.002	0.024	N/A	5.4
3E	57[a]	0.020	0.088	13, 17	4.9
4A	687	0.29	0.40	6, 11	7.4
4B	915	0.37	0.45	6-7, 12.5, 18	5.4
4C	809	0.34	0.46	6-7, 12.5, 18	4.6
4D	1297	0.54	0.73	6, 12	5.9
4E	641	0.28	0.47	6, 14	1.0

a) Surface area measured over P/P_o = 0.1-0.2 to give a linear fit to the BET equation. b) Includes pore diameters $\leq$ 20 Å. c) Weight percent at 1 bar and 298 K.

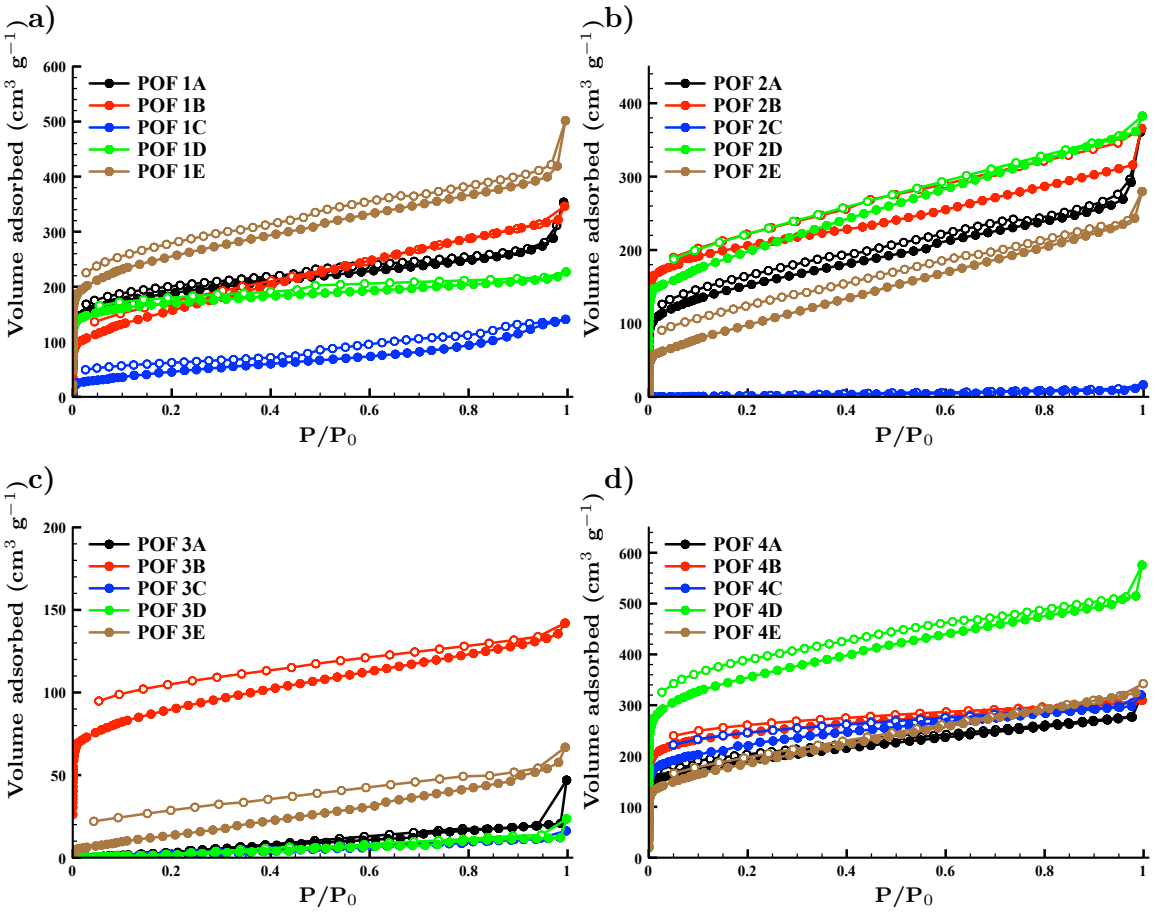

Fig. 3.3: *Nitrogen isotherms at 77 K for POFs a) 1A-1E; b) 2A-2E; c) 3A-3E; d) 4A-4E.*

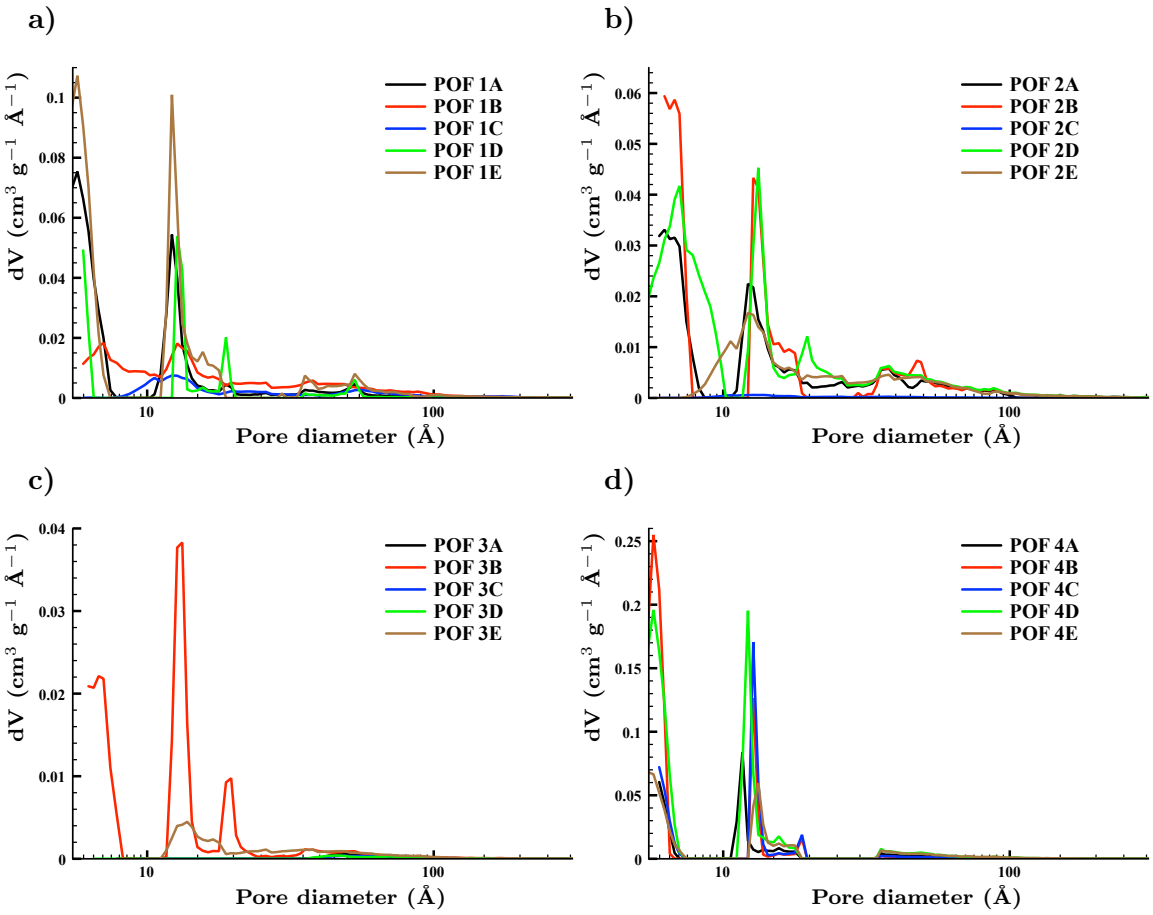

Fig. 3.4: *Pore size distributions from nitrogen isotherms at 77 K for POFs a) 1A-1E; b) 2A-2E; c) 3A-3E; d) 4A-4E.*

The total pore volume (V_{total}) and pore size distributions (Figure 3.4) were calculated from the N_2 isotherms using a carbon equilibrium slit/cylindrical model of non-local density functional theory (NLDFT) and are summarized in Table 3.1. The POFs with the highest surface areas and pore volumes have predominant pore sizes of 6-7 Å as well as 11-13 Å.

The influence of extending the monomer size by additional of a phenyl linkage unit on the surface area and pore volumes of the POFs is apparent. One instance of this is the comparison of triresorcinols **2** and **3** where **3** has the extended phenyl linkage. Polymers containing precursor **3** have lower yields and lower surface area properties compared to polymers containing precursor **2**. In fact, the only material in **POF 3A-3E** to have any appreciable BET surface area or micropore volume is **POF 3B** whereas **POFs 2A**, **2B**, and **2D** and **2E** all have moderate BET surface areas and micropore volumes. The larger size of precursor **3** compared to precursor **2** could result in more opportunities for interpenetration or π-stacking of the polymer. In addition, shifts in the predominant pore diameter occur; for a given aldehyde series, either the predominant pore diameter increases or more pore volume is found for larger pore diameters across the series of **1-3**. Concomitant with the shift in pore diameter, a decrease in total pore volume occurs in the series **1-3**. This trend is consistent with other reports on the influence of changing monomer strut size on BET surface area, pore diameter, and pore volume (Jiang *et al.*, 2008). The pore volumes for POFs containing **4** are larger because the tetrahedral monomer provides structural rigidity and fewer opportunities for interpenetration or π-stacking compared to the more planar monomers.

Whereas lower surface area properties were anticipated for **3** when comparing **2** versus **3**, the tetrahedral geometry of **D** and **E** is expected to be less sensitive to phenyl linkage expansion. The tetrahedral units should be less prone to phenyl-phenyl stacking that reduces the BET surface area and pore volume of the POFs. Indeed, the trend observed when looking at POFs containing **2** versus **3** does not translate to the comparison of POFs that contain **D** versus **E**. **POFs 2D**, **3D**, and **4D** have higher BET surface areas than **POFs 2E**, **3E**, and **4E**, respectively, while **POF 1E** has a larger surface area than **POF 1D**. However, a larger percentage of the total pore volume is microporous for **POF 1D** compared to **POF 1E**. The size matching of **1** and **D** is higher than that of **1** and **E** for ensuring a predominantly microporous material.

POFs containing the bent dialdehyde **C** have generally low surface areas and pore volumes. The moderate surface area properties of **POF 4C** are attributed to the geometry of precursor **4** and size matching of the **4C** precursor combination.

Looking at the summary of the surface area and pore volume properties of **POFs 1A-4E** in Table 3.1, the hypothesis that tetrahedral geometry is beneficial for making microporous materials and prohibiting interactions that reduce polymer surface area

(PEI *et al.*, 2014; STOCKEL *et al.*, 2009; YUAN *et al.*, 2011; ZHAO *et al.*, 2012) has been upheld. Additionally, the polymer architecture is sensitive to well-matched monomer size and complimentary geometries.

Gravimetric carbon dioxide isotherms were collected at 298 K for **POFs 1A-4E** and are shown in Figure B.11. The carbon dioxide uptake varies widely among this series of polymers from 1.0-9.0 % at 298 K and 1 bar. Accessible -OH groups of the phloroglucinol and resorcinol moieties were hypothesized to be advantageous for improved CO_2 capture through enhanced van der Waals (dipole-quadrupole) interaction compared to analogous materials without hydroxy groups (LING *et al.*, 2012). In addition, polymeric hydrogen bonding interactions may form additional microporous cavities that are suitable for low pressure CO_2 capture.

A summary of the CO_2 uptake at 298 K and 1 bar is given in Table 3.1. There are no significant correlations between the CO_2 uptake at 298 K and 1 bar and the N_2 surface area, micropore volume, or total pore volume of the POFs. For example, **POF 2B** and **POF 2D** both have similar micropore volumes. However, **POF 2B** has nearly twice the carbon dioxide capture capacity as **POF 2D** at 298 K and 1 bar. Similarly, **POF 4D** has 3.5 times the micropore volume as **POF 2E**, yet **POF 2E** has a larger CO_2 capture capacity compared to **POF 4D**, the POF with the largest micropore volume and BET surface area in the series. That said, the best performing materials (**POF 1D**, **POF 2B**, **POF 3B**, and **POF 4A**) have at non-trivial amount of micropore volume as measured by N_2 adsorption at 77 K. Accessible pore volume suitable for CO_2 capture may exist but cannot be detected by adsorption of N_2.

The isosteric heat of adsorption (Q_{st}) was measured for selected polymers to determine how well CO_2 "sticks" to the material. Using the Clausius-Clapeyron equation:

$$\ln \frac{P_1}{P_2} = \frac{Q_{st}}{R}\left(\frac{1}{T_2} - \frac{1}{T_1}\right) \tag{3.2}$$

where P is pressure, R is the gas constant, and T is temperature, values of Q_{st} for **POFs 1A**, **2A**, and **2B** were determined from Equation 3.2 and gravimetric CO_2 capture values at 273 K and 298 K (Figure 3.5). These values are shown in Table 3.2 and indicate physisorption is the dominant adsorption mechanism while the increase in Q_{st} at lower CO_2 loadings suggests enhanced physical adsorption within micropores occurs. The tertiary amine of **B** was anticipated to improve CO_2 capture through a minor chemisorptive contribution. However, this is not suggested by the Q_{st} of **POF 2B** compared to **POF 1A** or **POF 2A** at 1.0 wt. % loading.

As suggested by Snurr and coworkers (WILMER *et al.*, 2012), materials with pore diameters no larger than 6 Å, surface areas 1000-2000 $m^2\ g^{-1}$, and heats of adsorption around 30 kJ mol^{-1} are best for flue gas adsorbents. Beyond these inexact parameters, there is no *a priori* knowledge to suggest there should be a correlation between carbon capture capacity and the subtle geometric and chemical differences of the polymers

Table 3.2: *Q_{st} (kJ mol^{-1}) at various CO_2 loadings (wt. %) for **POFs 1A**, **2A**, and **2B**. Values of Q_{st} are calculated from Figure 3.5 and Equation 3.2.*

	Q_{st} (1.0 wt. %)	Q_{st} (2.2 wt. %)	Q_{st} (5.6 wt. %)
POF 1A	39.1	37.0	33.2
POF 2A	46.4	33.2	28.2
POF 2B	40.2	31.9	31.0

presented in this work. Other adsorbent evaluation criteria such as regenerability, working capacity, and selectively vary for carbon capture applications and are also only loosely associated with pore property and chemical functionality. However, this first generation of phloroglucinol and resorcinol POF materials are in or near the range of the above criteria for desired carbon capture materials.

4 Conclusions

New porous polymeric organic frameworks made from monomers rich in hydroxy groups have been synthesized and fully characterized. We have shown that a synthesis procedure prescribed for the synthesis of phloroglucinol POFs can be extended to resorcinol monomers without the inclusion of acid or base catalysts as required for synthesizing resorcinol-formaldehyde aerogels. Because the exact extended structures of these materials are unknown, it is difficult to correlate the interplay of metrics such as accessible pore volume and chemical functionality (e.g. number of hydroxy groups) to CO_2 capture capacity. However, this systematic study of polymers containing monomers of various sizes and geometries indicates POFs are incredibly sensitive to the physical structure of the monomer as well as the pairing of co-monomers. We have further confirmed that precursors of particular molecular design perform better than others, in particular those with tetrahedral centers and co-monomers that are well-matched in size. POFs containing resorcinol derivatives perform as well as if not better than the phloroglucinol analogs, and the resorcinol moiety contains a wealth of synthetic and structural tunability.

For the first time, the systematic investigation of the influence of monomer design on POFs made from tri- and tetraresorcinols and benzaldehydes has been reported. The ease of synthesis and favorable surface areas make this class of resorcinol POFs promising materials for future exploration of applications in addition to CO_2 capture. Current efforts are underway exploring the post-synthetic modification of phloroglucinol and resorcinol POFs for improved CO_2 capture capacity and pore size modulation.

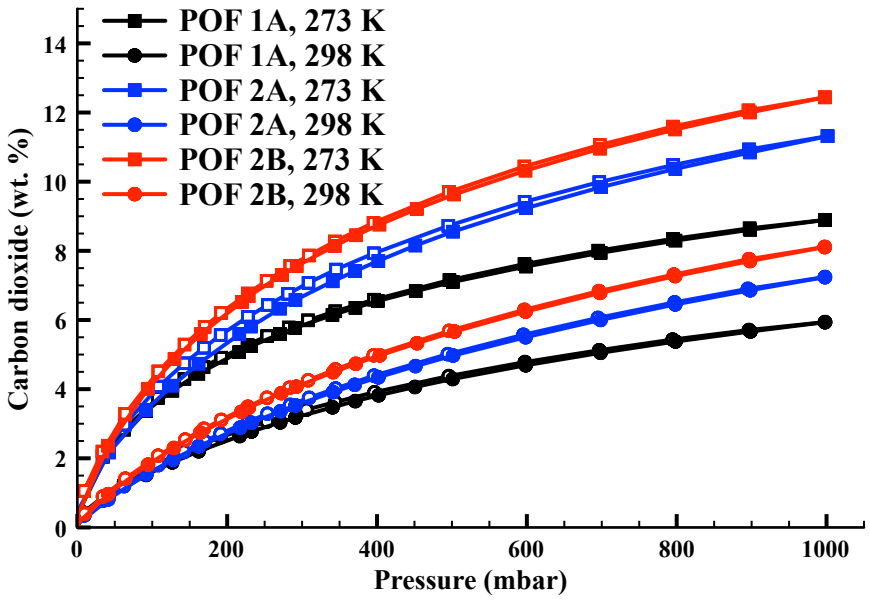

Fig. 3.5: *Gravimetric CO_2 adsorption (filled trace) and desorption (open trace) for **POF 1A** (black), **POF 2A** (blue), and **POF 2B** (red) at 273 K (square) and 298 K (circle).*

Acknowledgments

This work was partially supported by the Laboratory Director's Research and Development program of the Oak Ridge National Laboratory (ORNL) which is managed by UT-Battelle, LLC for the US Department of Energy (DOE) under contract No. DE-AC05-00OR22725. We thank Dr. Ed Hagaman for collecting the ^{13}C solid state NMR spectra.

A Appendix: Synthetic details

Tetrakis(4'-formyl-[1,1'-biphenyl]-4-yl)methane (**E**):

A deoxygenated solution of 1 M Na_2CO_3 (20 mL) was transferred *via* syringe to a degassed suspension of tetrakis(4-bromophenyl)methane (1.00 g, 1.57 mmol), 4-formylphenylboronic acid (1.13 g, 7.53 mmol), and $Pd(dppf)Cl_2 \cdot CH_2Cl_2$ (0.151 g, 0.183 mmol) in 1:1 toluene/methanol (50 mL). The mixture was refluxed for 48 hours. After cooling to room temperature, the reaction mixture was extracted with CH_2Cl_2 (5 x 40 mL). The organic layers were combined, dried over $MgSO_4$, filtered, and evaporated to dryness. The crude product was precipitated from hot DMF to give the title compound as a white solid in 62 % yield. ^{1}H NMR (400 MHz, $CDCl_3$): δ 10.06 (s, 4H), 7.96 (d, J = 8 Hz, 8H), 7.79 (d, J = 8 Hz, 8H), 7.63 (d, J = 8 Hz, 8H), 7.47 (d, J = 8 Hz, 8H) ^{13}C NMR (100 MHz, $CDCl_3$): δ 191.7, 146.6, 146.3, 137.4, 135.2, 131.5, 130.2, 127.4, 126.6, 64.3.

5''-(3',5'-Dimethoxy[1,1'-biphenyl]-4-yl)-3,3'''',5,5''''-tetramethoxy-1,1':4',1'':3'',1''':4''',1'''':quinquephenyl:

A deoxygenated solution of 1 M Na_2CO_3 (20 mL) was transferred *via* syringe to a degassed suspension of 1,3,5-tris(4-bromophenyl)benzene (0.50 g, 0.92 mmol), 3,5-dimethoxyphenylboronic acid (0.60 g, 3.3 mmol), and $Pd(dppf)Cl_2 \cdot CH_2Cl_2$ (0.064 g, 0.078 mmol) in 2:1 toluene/methanol (60 mL). The mixture was refluxed for 40 hours. After cooling to room temperature, the reaction mixture rotary evaporated to remove most of the toluene/methanol solvent mixture. The residue was extracted with CH_2Cl_2 (3 $\times$ 20 mL). The organic layers were combined, dried over $MgSO_4$, filtered, and evaporated to dryness. The crude product was purified *via* column chromatography on silica with 4:1 CH_2Cl_2/hexanes as the eluent to give a white solid in 66 % yield. ^{1}H NMR (400 MHz, $CDCl_3$): δ 7.90 (s, 3H), 7.81 (d, J = 8.4 Hz, 6H), 7.73 (d, J = 8.0 Hz, 6H), 6.83 (d, J = 2.4 Hz, 6H), 6.52 (t, J = 2.4 Hz, 3H), 3.89 (s, 18H). ^{13}C NMR (100 MHz, $CDCl_3$): δ 161.1, 142.9, 142.0, 140.5, 140.3, 127.7, 125.0, 105.4, 99.4, 55.4.

5''-(3',5'-Dihydroxy[1,1'-biphenyl]-4-yl)-[1,1':4',1'':3'',1''':4''',1''''-quinquephenyl]-3,3'''',5,5''''-tetrol (**3**):

BBr_3 (1 M in CH_2Cl_2, 3.3 mL) was added dropwise to a -80 ℃ solution of 5''-(3',5'-dimethoxy[1,1'-biphenyl]-4-yl)-3,3'''',5,5''''-tetramethoxy-1,1':4',1'':3'',1''':4''',1''''-quinquephenyl (0.34 g, 0.47 mmol) in anhydrous CH_2Cl_2 (15 mL). The mixture was allowed to warm to room temperature overnight. Deionized water (10 mL) was added slowly fol-

lowed by 1 M NaOH until a biphasic solution with no discernible solids had formed. The aqueous layer was collected, and the organic layer was extracted with 0.1 M NaOH (2 × 10 mL). 2 M HCl was added to the combined aqueous layers until a precipitate formed. The suspension was filtered, washed with water (3 × 15 mL), and dried *in vacuo* at 70 ℃ to afford a light brown solid in 93 % yield. ^{1}H NMR (400 MHz, $(CD_3)_2CO$): δ 8.38 (s, 6H), 8.04 (s, 3H), 7.97 (d, J = 8.4 Hz, 6H), 7.74 (d, J = 8.4 Hz, 6H), 6.72 (d, J = 2.4 Hz, 6H), 6.41 (t, J = 2.4 Hz, 3H). ^{13}C NMR (100 MHz, $(CD_3)_2CO$): δ 160.0, 143.6, 142.9, 141.5, 140.8, 128.6, 128.2, 125.4, 106.4, 102.8.

B Appendix: Characterization results

NMR spectra, infrared spectra, TGA traces, UV-Vis-NIR diffuse reflectance spectra, SEM images, and gravimetric CO_2 isotherms.

Table A.1: *Reagent amounts, solvent volume, and isolated yield for POFs* ***1A-4E***

POF	Precursor	Mass (g)	Moles (mmol)	Precursor	Mass (g)	Moles (mmol)	Dioxane (mL)	Yield (%)
1A	**1**	0.504	4.00	**A**	0.402	3.00	5	90
1B	**1**	0.252	2.00	**B**	0.329	2.00	5	73
1C	**1**	0.098	0.77	**C**	0.167	0.583	3	72
1D	**1**	0.200	1.58	**D**	0.257	0.594	4	78
1E	**1**	0.050	0.40	**E**	0.110	0.149	6	71
2A	**2**	0.234	0.582	**A**	0.059	0.44	6	82
2B	**2**	0.160	0.398	**B**	0.064	0.19	3	74
2C	**2**	0.103	0.256	**C**	0.054	0.19	5	48
2D	**2**	0.151	0.376	**D**	0.061	0.14	5	56
2E	**2**	0.103	0.256	**E**	0.070	0.095	6	67
3A	**3**	0.102	0.162	**A**	0.016	0.12	5	36
3B	**3**	0.101	0.160	**B**	0.026	0.079	6	73
3C	**3**	0.102	0.162	**C**	0.034	0.12	4	31
3D	**3**	0.101	0.160	**D**	0.026	0.060	4	28
3E	**3**	0.103	0.163	**E**	0.044	0.060	6	43
4A	**4**	0.300	0.398	**A**	0.054	0.40	5	91
4B	**4**	0.106	0.141	**B**	0.030	0.091	6	47
4C	**4**	0.096	0.13	**C**	0.037	0.13	4	20
4D	**4**	0.125	0.166	**D**	0.036	0.083	4	75
4E	**4**	0.235	0.312	**E**	0.115	0.156	5	31

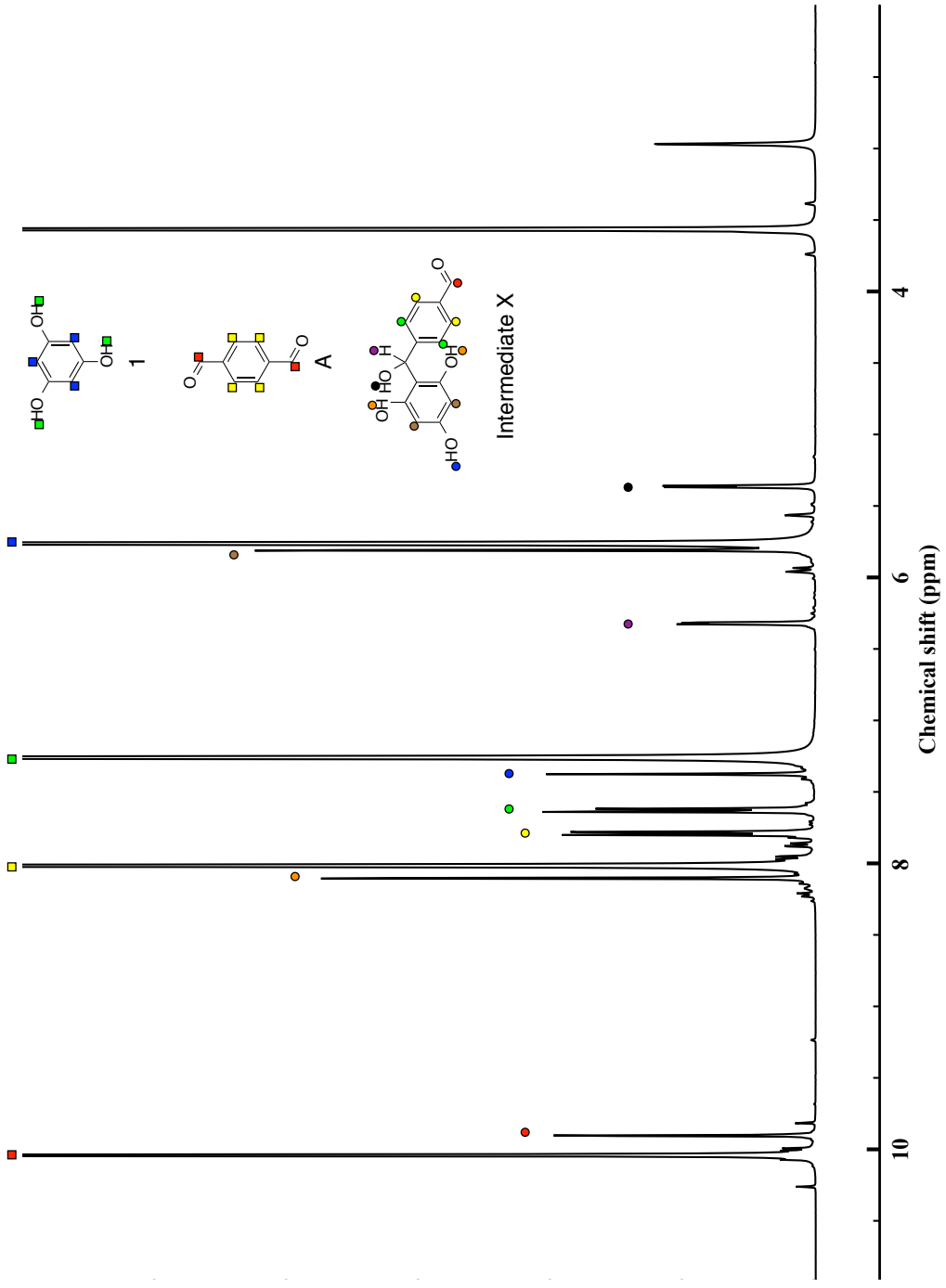

Fig. B.1: ^{1}H *NMR spectrum (70 °C, 1,4-dioxane-d*$_8$*) of phloroglucinol and terephthalaldehyde after treatment at 70 °C for one hour. The resonances associated with phloroglucinol, terephthaldehyde, and intermediate X have been assigned.*

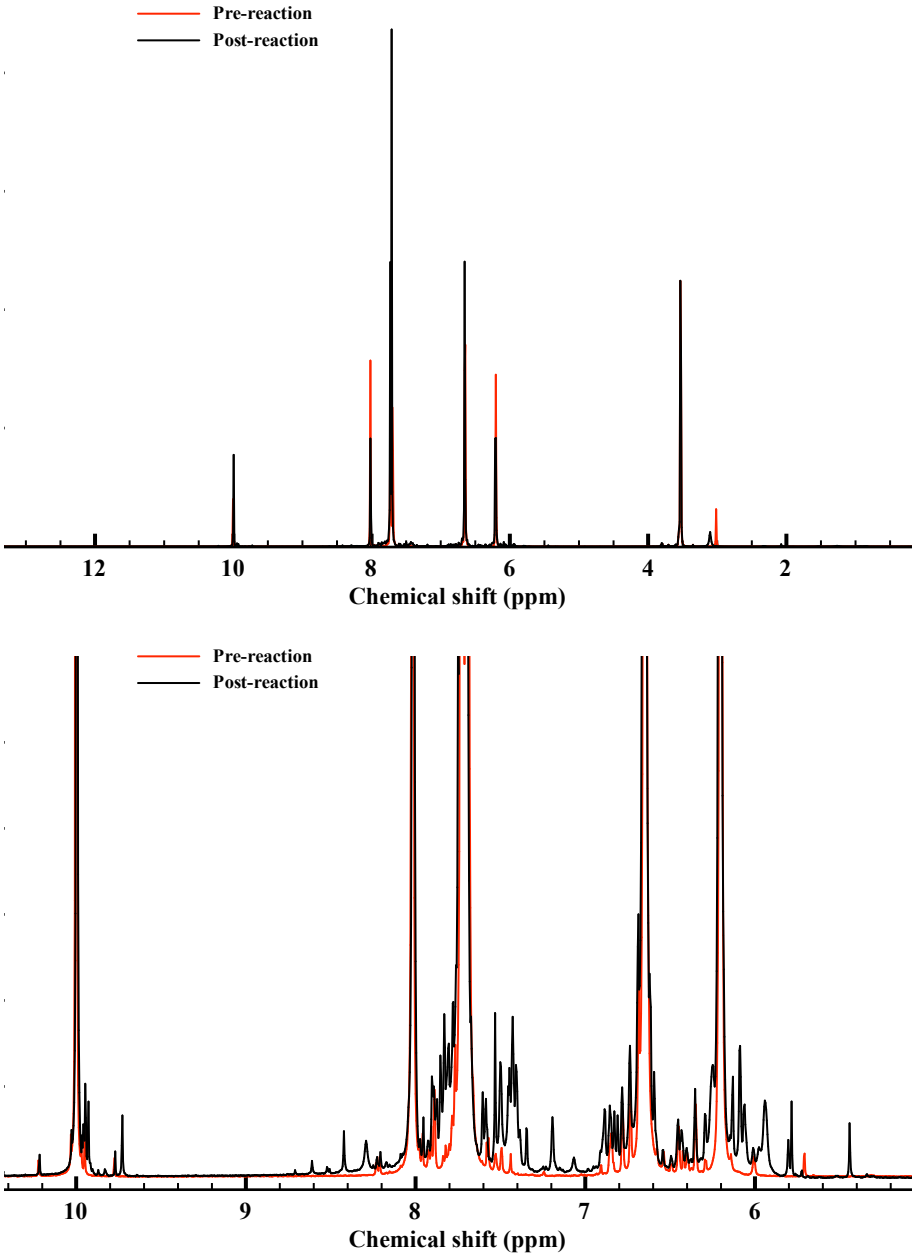

Fig. B.2: ^{1}H *NMR spectra of* ***2*** *and* ***A*** *in 1,4-dioxane-*d_8 *before (red) and after (black) treatment at 220 ℃ for one hour in a sealed vessel. Spectra were collected at room temperature.*

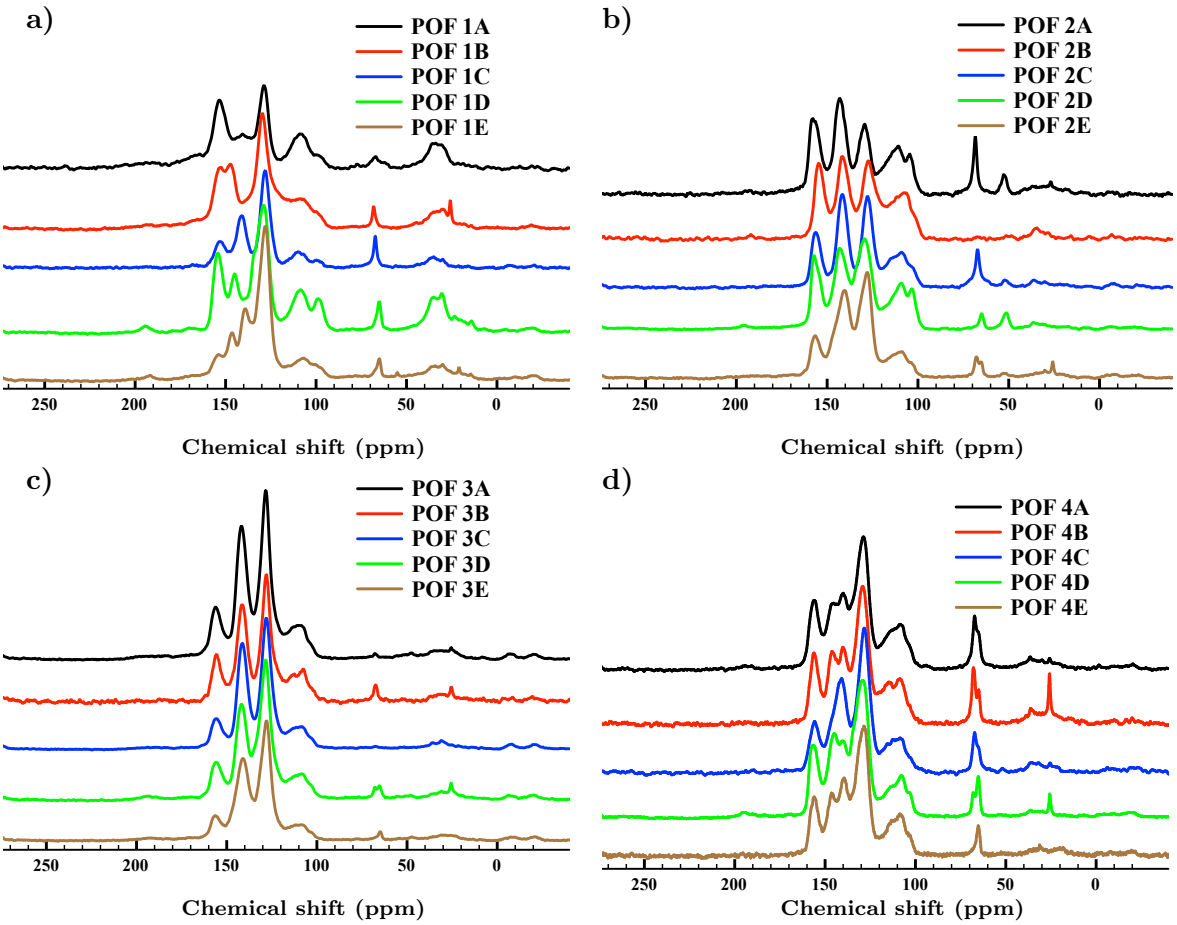

Fig. B.3: *Solid state* ^{13}C *NMR of POFs a) 1A-1E; b) 2A-2E; c) 3A-3E; d) 4A-4E.*

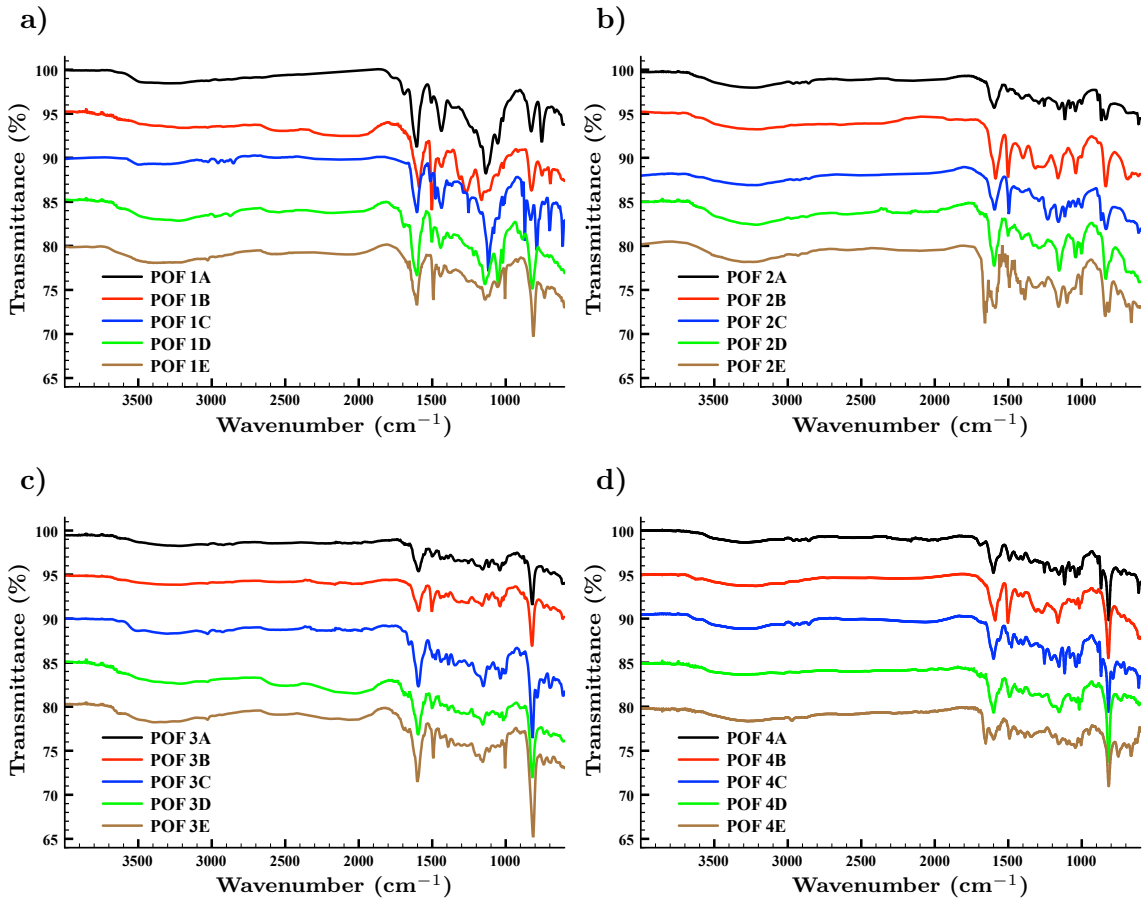

Fig. B.4: *Infrared spectra for POFs a) 1A-1E; b) 2A-2E; c) 3A-3E; d) 4A-4E.*

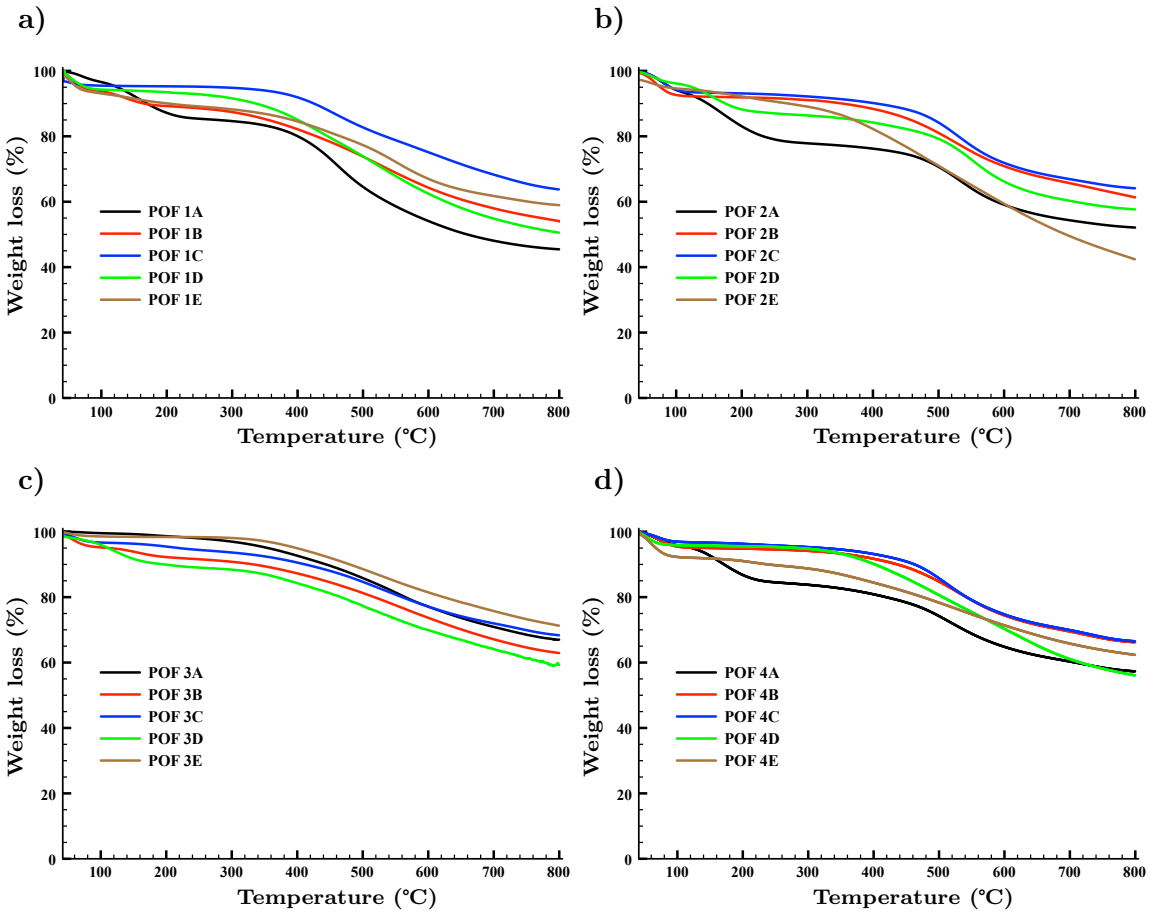

Fig. B.5: *Thermogravimetric analysis traces for POFs a) 1A-1E; b) 2A-2E; c) 3A-3E; d) 4A-4E.*

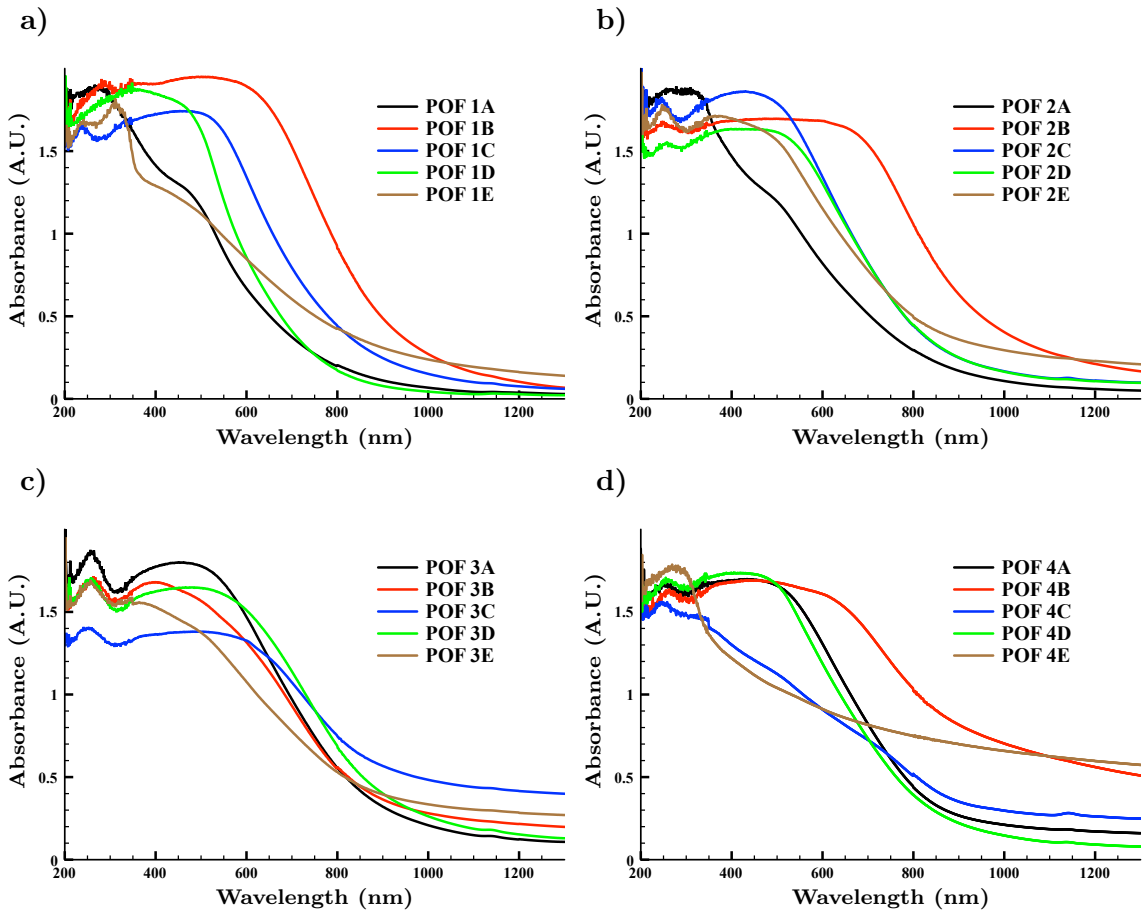

Fig. B.6: *Diffuse reflectance traces for POFs a) 1A-1E; b) 2A-2E; c) 3A-3E; d) 4A-4E.*

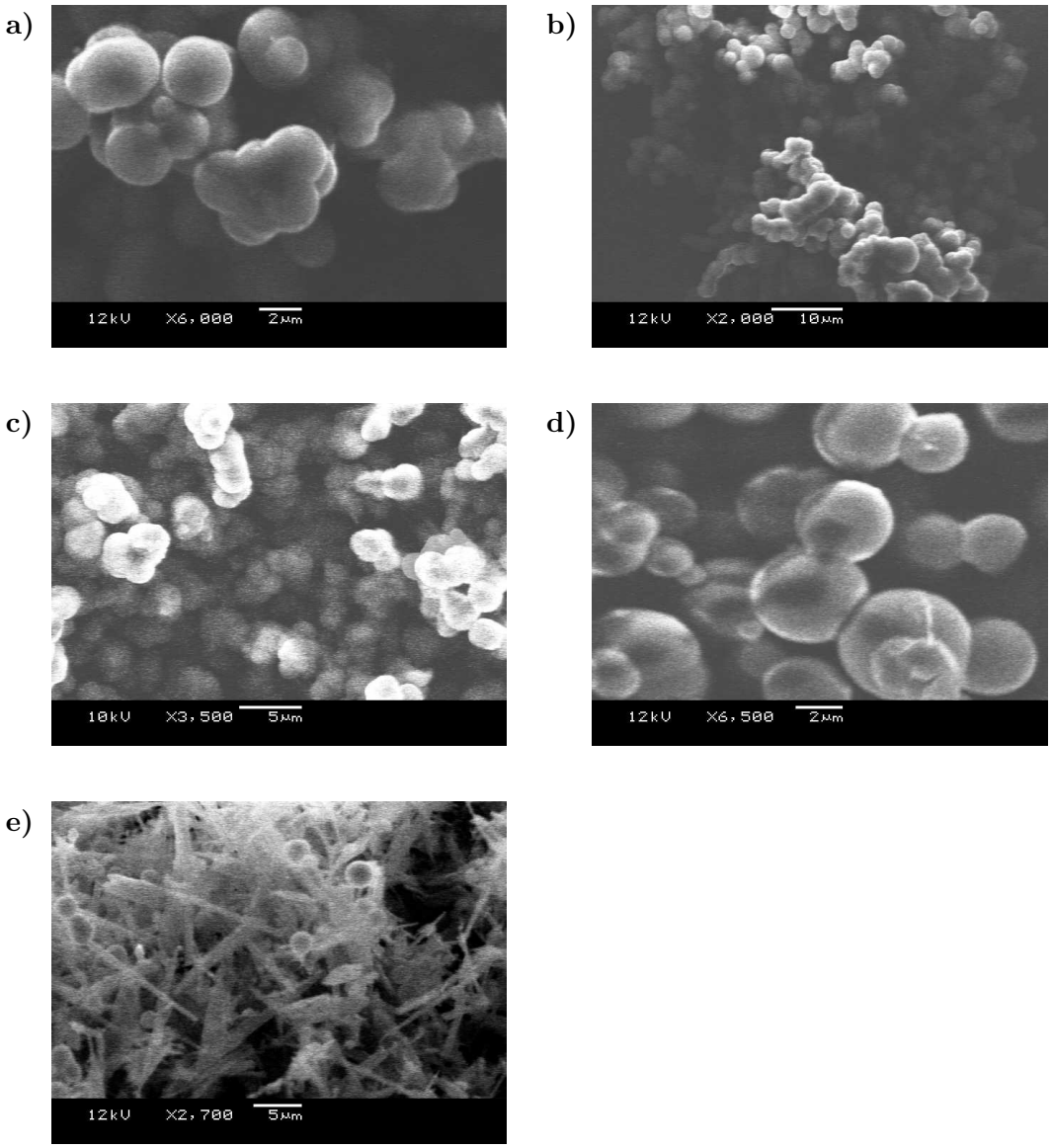

Fig. B.7: *SEM images of POFs 1A-E.*

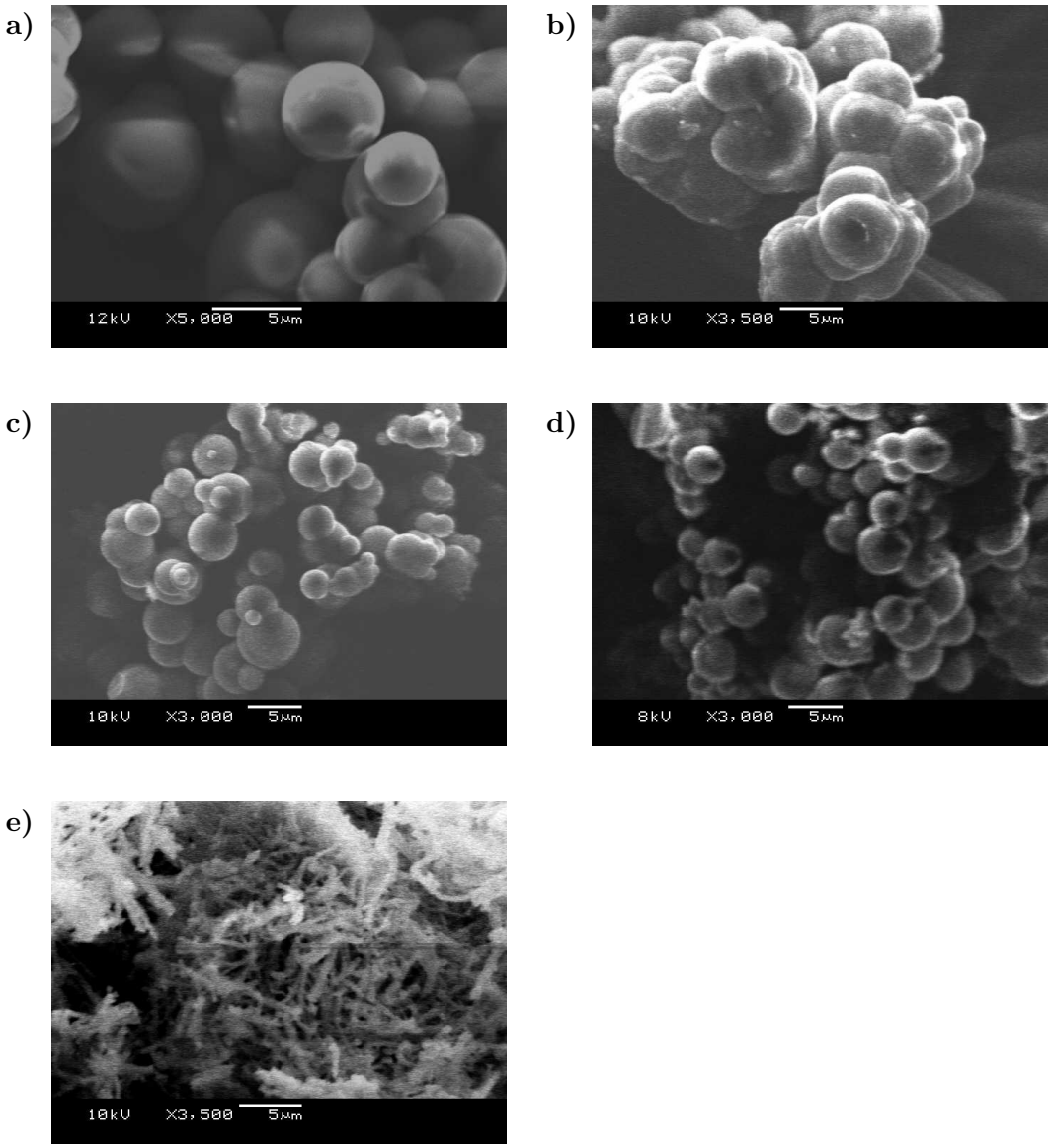

Fig. B.8: *SEM images of POFs 2A-E.*

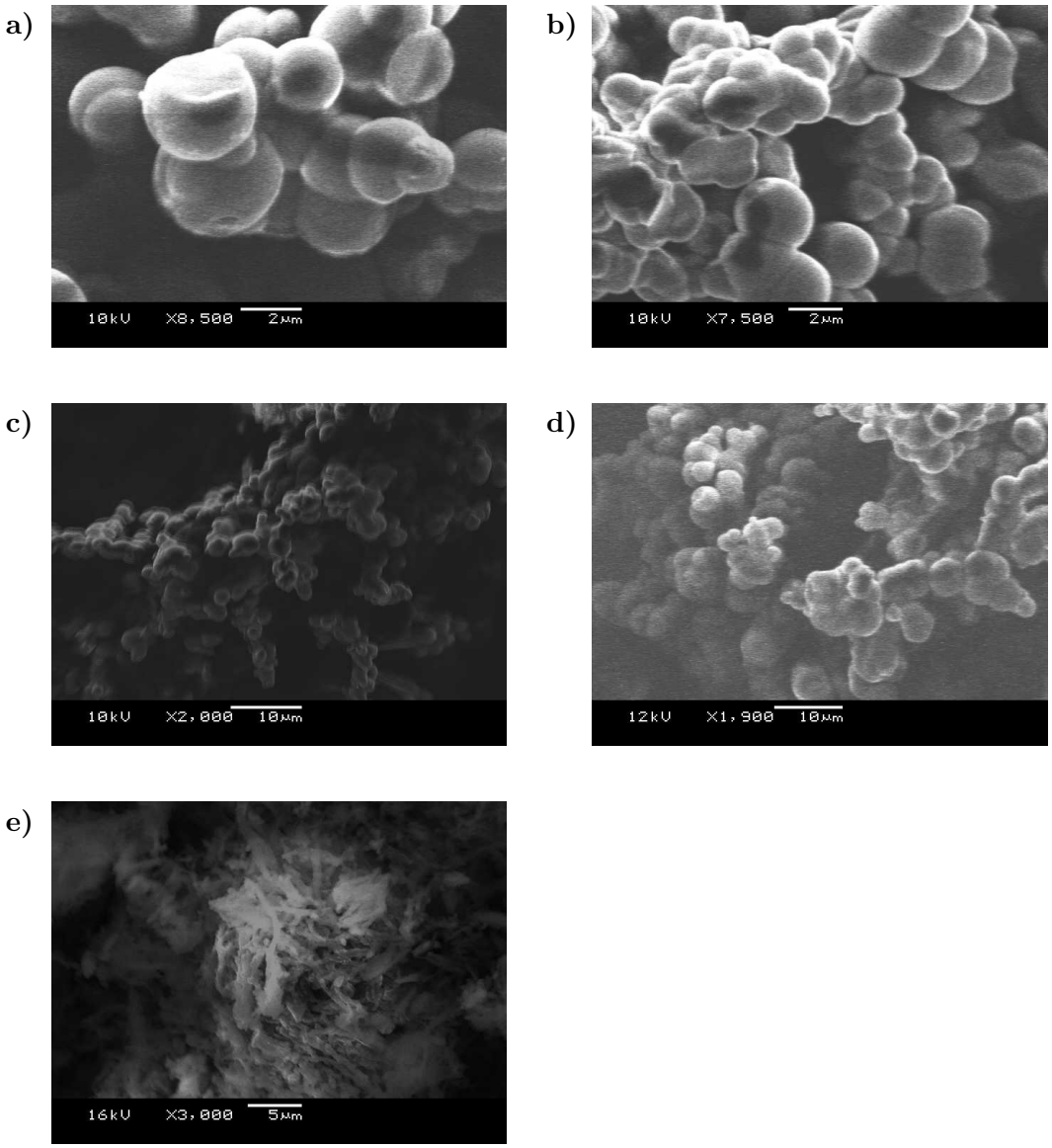

Fig. B.9: *SEM images of POFs 3A-E.*

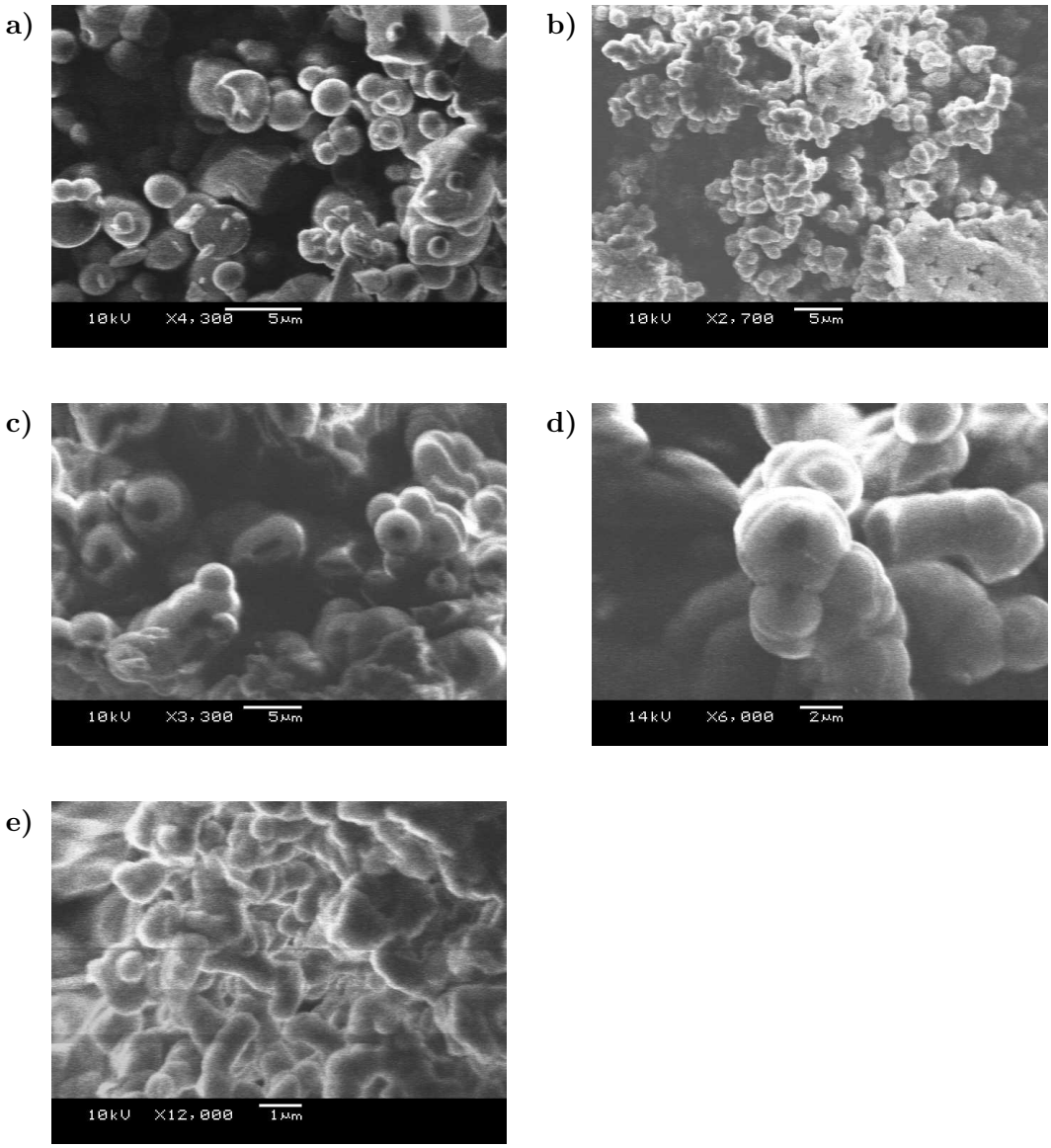

Fig. B.10: *SEM images of POFs 4A-E.*

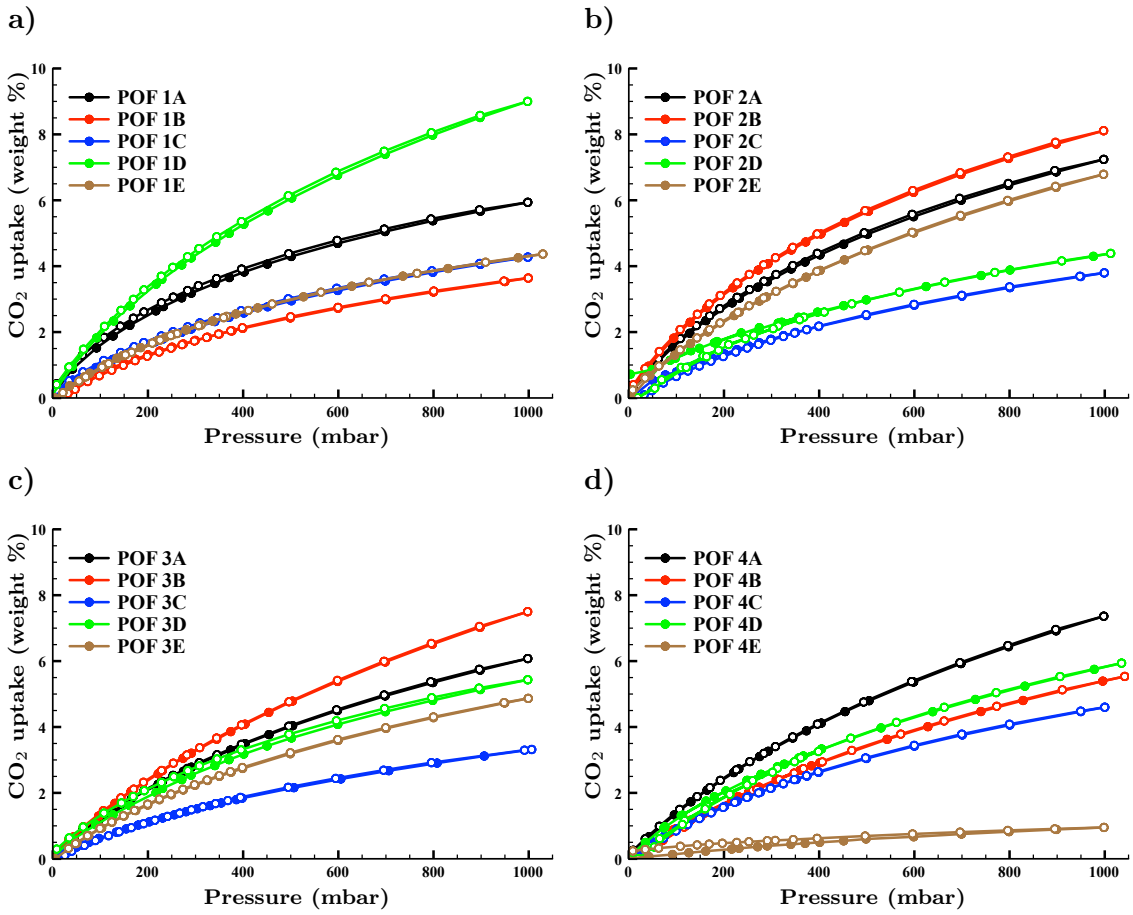

Fig. B.11: *Carbon dioxide isotherms at 298 K for POFs a) 1A-1E; b) 2A-2E; c) 3A-3E; d) 4A-4E.*

References

BAE, Y.-S., YAZAYDIN, A. O., AND SNURR, R. Q. **2010** Evaluation of the BET method for determining surface areas of mofs and zeolites that contain ultra-micropores. *Langmuir* **26**(8) 5475–5483.

BUDD, P. M., GHANEM, B. S., MAKHSEED, S., MCKEOWN, N. B., MSAYIB, K. J., AND TATTERSHALL, C. E. **2004** Polymers of intrinsic microporosity (PIMs): Robust, solution-processable, organic nanoporous materials. *Chem. Commun.* pages 230–231.

CHAUMONT, C., MOBIAN, P., KYRITSAKAS, N., AND HENRY, M. **2013** Synthesis, topology and energy analysis of crystalline resorcinol-based oligophenylene molecules with various symmetries. *Cryst. Eng. Comm.* **15** 6845–6862.

CHOI, S., DRESE, J. H., EISENBERGER, P. M., AND JONES, C. W. **2011** Application of amine-tethered solid sorbents for direct CO_2 capture from the ambient air. *Environ. Sci. Technol.* **45**(6) 2420–2427.

DING, S.-Y. AND WANG, W. **2013** Covalent organic frameworks (COFs): From design to applications. *Chem. Soc. Rev.* **42** 548–568.

FARHA, O. K., ERYAZICI, I., JEONG, N. C., HAUSER, B. G., WILMER, C. E., SARJEANT, A. A., SNURR, R. Q., NGUYEN, S. T., YAZAYDIN, A. O., AND HUPP, J. T. **2012** Metal–organic framework materials with ultrahigh surface areas: Is the sky the limit? *J. Am. Chem. Soc.* **134**(36) 15016–15021.

FOURNIER, J.-H., WANG, X., AND WUEST, J. D. **2003** Derivatives of tetraphenylmethane and tetraphenylsilane: Synthesis of new tetrahedral building blocks for molecular construction. *Can. J. Chem.* **81**(5) 376–380.

GAO, X., ZOU, X., MA, H., MENG, S., AND ZHU, G. **2014** Highly selective and permeable porous organic framework membrane for CO_2 capture. *Adv. Mater.* **26**(22) 3644–3648.

GASSENSMITH, J. J., FURUKAWA, H., SMALDONE, R. A., FORGAN, R. S., BOTROS, Y. Y., YAGHI, O. M., AND STODDART, J. F. **2011** Strong and reversible binding of carbon dioxide in a green metal–organic framework. *J. Am. Chem. Soc.* **133**(39) 15312–15315.

HORIKAWA, T., HAYASHI, J., AND MUROYAMA, K. **2004** Size control and characterization of spherical carbon aerogel particles from resorcinol–formaldehyde resin. *Carbon* **42**(1) 169 – 175.

Jiang, J.-X., Su, F., Trewin, A., Wood, C. D., Niu, H., Jones, J. T. A., Khimyak, Y. Z., and Cooper, A. I. **2008** Synthetic control of the pore dimension and surface area in conjugated microporous polymer and copolymer networks. *J. Am. Chem. Soc.* **130**(24) 7710–7720.

Katsoulidis, A. P. and Kanatzidis, M. G. **2011** Phloroglucinol based microporous polymeric organic frameworks with oh functional groups and high co2 capture capacity. *Chem. Mater.* **23**(7) 1818–1824.

Kaur, P., Hupp, J. T., and Nguyen, S. T. **2011** Porous organic polymers in catalysis: Opportunities and challenges. *ACS Catal.* **1**(7) 819–835.

Kuhnert, N., Patel, C., and Jami, F. **2005** Synthesis of chiral nonracemic polyimine macrocycles from cyclocondensation reactions of biaryl and terphenyl aromatic dicarboxaldehydes and 1R,2R-diaminocyclohexane. *Tetrahedron Lett.* **46**(44) 7575 – 7579.

Lässig, D., Lincke, J., Moellmer, J., Reichenbach, C., Moeller, A., Gläser, R., Kalies, G., Cychosz, K. A., Thommes, M., Staudt, R., and Krautscheid, H. **2011** A microporous copper metal–organic framework with high H_2 and CO_2 adsorption capacity at ambient pressure. *Angew. Chem. Int. Ed.* **50**(44) 10344–10348.

Lee, S.-Y. and Park, S.-J. **2015** A review on solid adsorbents for carbon dioxide capture. *J. Ind. Eng. Chem.* **23** 1–11.

Li, G. and Wang, Z. **2013** Microporous polyimides with uniform pores for adsorption and separation of co2 gas and organic vapors. *Macromolecules* **46**(8) 3058–3066.

Li, G., Zhang, B., Yan, J., and Wang, Z. **2014a** Micro- and mesoporous poly(schiff-base)s constructed from different building blocks and their adsorption behaviors towards organic vapors and CO_2 gas. *J. Mater. Chem. A* **2** 18881 – 18888.

Li, G., Zhang, B., Yan, J., and Wang, Z. **2014b** Tetraphenyladamantane-based polyaminals for highly efficient captures of co2 and organic vapors. *Macromolecules* **47**(19) 6664 – 6670.

Ling, Y., Yang, F., Deng, M., Chen, Z., Liu, X., Weng, L., and Zhou, Y. **2012** Novel iso-reticular zn(ii) metal-organic frameworks constructed by trinuclear-triangular and paddle-wheel units: Synthesis, structure and gas adsorption. *Dalton Trans.* **41** 4007–4011.

LIU, Y., WANG, Z. U., AND ZHOU, H.-C. **2012** Recent advances in carbon dioxide capture with metal-organic frameworks. *Greenhouse Gas Sci Technol.* **2**(4) 239–259.

LU, W., SCULLEY, J. P., YUAN, D., KRISHNA, R., AND ZHOU, H.-C. **2013** Carbon dioxide capture from air using amine-grafted porous polymer networks. *J. Phys. Chem. C* **117**(8) 4057–4061.

MA, J., WANG, M., DU, Z., CHEN, C., GAO, J., AND XU, J. **2012** Synthesis and properties of furan-based imine-linked porous organic frameworks. *Polym. Chem.* **3** 2346–2349.

MA, X., LI, Y., CAO, M., AND HU, C. **2014** A novel activating strategy to achieve highly porous carbon monoliths for CO_2 capture. *J. Mater. Chem. A* **2** 4819–4826.

MCKEOWN, N. B. AND BUDD, P. M. **2006** Polymers of intrinsic microporosity (PIMs): Organic materials for membrane separations, heterogeneous catalysis and hydrogen storage. *Chem. Soc. Rev.* **35** 675–683.

PEI, C., BEN, T., LI, Y., AND QIU, S. **2014** Synthesis of copolymerized porous organic frameworks with high gas storage capabilities at both high and low pressures. *Chem. Commun.* **50** 6134–6136.

ROUQUEROL, J., LLEWELLYN, P., AND ROUQUEROL, F. **2007** Is the BET equation applicable to microporous adsorbents? In P. LLEWELLYN, F. RODRIQUEZ-REINOSO, J. ROUQEROL, AND N. SEATON, editors, *Characterization of Porous Solids VII*, volume 160 of *Studies in Surface Science and Catalysis*, pages 49 – 56. Elsevier.

SIMALOU, O., LU, R., XUE, P., GONG, P., AND ZHANG, T. **2014** C3-symmetrical cyano-substituted triphenylbenzenes for organogels and organic nanoparticles with controllable fluorescence and aggregation-induced emission. *Eur. J. Org. Chem.* **0**(14) 2907–2916.

STOCKEL, E., WU, X., TREWIN, A., WOOD, C. D., CLOWES, R., CAMPBELL, N. L., JONES, J. T., KHIMYAK, Y. Z., ADAMS, D. J., AND COOPER, A. I. **2009** High surface area amorphous microporous poly(aryleneethynylene) networks using tetrahedral carbon- and silicon-centred monomers. *Chem. Commun.* pages 212–214.

THOMMES, M., KANEKO, K., NEIMARK, A. V., OLIVIER, J. P., RODRIGUEZ-REINOSO, F., ROUQUEROL, J., AND SING, K. S. W. **2015** Physisorption of gases,

with special reference to the evaluation of surface area and pore size distribution (IUPAC technical report). *Pure Appl. Chem.* **87**(9-10) 1051–1069.

Wilmer, C. E., Farha, O. K., Bae, Y.-S., Hupp, J. T., and Snurr, R. Q. **2012** Structure-property relationships of porous materials for carbon dioxide separation and capture. *Energy Environ. Sci.* **5** 9849–9856.

Yuan, D., Lu, W., Zhao, D., and Zhou, H.-C. **2011** Highly stable porous polymer networks with exceptionally high gas-uptake capacities. *Adv. Mater.* **23**(32) 3723–3725.

Zhang, M., Bosch, M., Gentle III, T., and Zhou, H.-C. **2014a** Rational design of metal-organic frameworks with anticipated porosities and functionalities. *Cryst. Eng. Comm.* **16** 4069–4083.

Zhang, X., Lu, J., and Zhang, J. **2014b** Porosity enhancement of carbazolic porous organic frameworks using dendritic building blocks for gas storage and separation. *Chem. Mater.* **26**(13) 4023–4029.

Zhao, Y.-C., Wang, T., Zhang, L.-M., Cui, Y., and Han, B.-H. **2012** Facile approach to preparing microporous organic polymers through benzoin condensation. *ACS Appl. Mater. Interfaces* **4**(12) 6975–6981.

Zou, X., Ren, H., and Zhu, G. **2013** Topology-directed design of porous organic frameworks and their advanced applications. *Chem. Commun.* **49** 3925–3936.